scientific reports

Check for updates

OPEN

Pumice soil stabilisation using alkali-activated waste glass for sustainable road subgrade applications

Roohollah Kalatehjari[1]✉, Elmira Khaksar Najafi[2] & Afshin Asadi[3]

This research explores the development of glass-based alkali-activated cement (GBAAC) for stabilising New Zealand pumice sand as a subgrade in road construction. Using GBAAC in road construction offers a sustainable solution by reducing waste glass (WG) accumulation in landfills and providing an effective alternative to conventional chemical soil stabilisers. Several mixtures were prepared by systematically optimising both the activator-to-precursor ratio (A/P), using a 10 M KOH solution as the activator, and the particle size distribution of the WG precursor to achieve optimal strength and performance characteristics. The maximum compressive strength of 37.9 MPa was obtained at an A/P of 0.4 after curing at 65 °C for 48 h. The microstructural analysis confirmed the formation of alkali/earth-alkali-silicate-hydrate gels involving Na^+, K^+, Ca^{2+}, and Mg^{2+} ions. An interesting aging phenomenon was observed, with compressive strength decreasing at 28 days due to depolymerisation, then surpassing initial strength at 56 days. Initial curing at 65 °C for 48 h resulted in a 56-day strength 2.6 times higher than that achieved with room temperature curing. An unground-to-ground WG unit ratio was selected as the optimal precursor composition, balancing strength requirements and production efficiency. California Bearing Ratio (CBR) tests demonstrated that mechano-chemical stabilisation using GBAAC significantly enhanced the stress-strain behaviour of pumice sand. The highest average CBR5.0 value of 64.70% was achieved with heavy compaction of GBAAC-stabilised samples, a substantial improvement from 21.67% for lightly compacted untreated samples.

Keywords Waste glass, Pumice soil, Glass-based alkali-activated cement, California bearing ratio, Compressive strength

Pumice soils, composed of light and porous volcanic rocks, are widespread in New Zealand, covering several areas of the central North Island, particularly along the lower Waikato River valley and parts of the Bay of Plenty[1,2]. These soils primarily consist of sandy to gravelly pumice materials, characterised by weak weathering and low clay content[3]. One of the main challenges associated with pumice soils is their low strength, which can render them incapable of supporting heavy loads, leading to excessive settlement and pavement damage. The crushing strength of pumice soils is significantly lower than that of hard-grained soils, highlighting their high crushability[4].

Another critical issue is the susceptibility of pumice soils to erosion, which can result in particle loss and compromise pavement stability. These soils are particularly vulnerable to water erosion, and, without adequate protection, heavy rainstorms can cause severe erosion[3], posing substantial challenges in road and transportation infrastructure. Stabilising the subgrade is therefore essential when working with pumice soils, as it improves the bearing capacity of the pavement and reduces the risk of failure[5].

In an era of increasing environmental concerns, sustainability is essential across all industries, including construction. Alkali-activated binders present a viable alternative to Portland cement for soil stabilisation, particularly in road construction[6,7]. Portland cement production contributes 5–8% of global CO_2emissions, projected to rise to 12–35% by 2050[8,9]. Alkali-activated cement (AAC), however, can reduce CO_2emissions associated with Portland cement production by up to 80%[10].

[1]Built Environment Engineering Department, School of Future Environments, Auckland University of Technology, Auckland 1010, New Zealand. [2]James Watt School of Engineering, University of Glasgow, Glasgow, UK. [3]EnvoGeotechnique Ltd., Auckland, New Zealand. ✉email: r.kalatehjari@aut.ac.nz

An expanding range of by-products and industrial wastes have shown promise as precursors or additives in AAC for soil stabilisation. Sugarcane bagasse ash, for example, is abundant in reactive silica and has been shown to strengthen weak or problematic soils and a sustainable solution for subgrade improvement under alkaline conditions[11–13]. Similarly, rice husk ash is another silica-rich resource that reacts favourably alone or with other precursors such as eggshell or carbide lime to produce AAC for stabilisation of a wide range of soil types[14–16]. Palm oil fuel ash has also been successfully used as precursor alone or with other materials such as magnesium oxide and cement for stabilisation of soft soil and subgrade by several researchers[17–21].

Industrial wastes and by-products such as steel slag, ground granulated blast furnace slag (GGBS), fly ash, and silica fume have drawn attention as favourable precursors due to their notable calcium, aluminium, and silica contents[22,23]. When blended with each other or other materials such as lime and cement, these materials shown effectiveness in soil stabilisation[23–27]. Another industrial waste is red mud, a residue from bauxite refining, that has proven successful in soil stabilisation as sole precursor or in combination with other materials such as GGBS, bottom ash, and cement[28–31]. Sewage sludge-based AAC has also been successfully applied in the stabilisation of both cohesive and granular soils[32–34]. Apart from agricultural and industrial by-products, a variety of minerals has been investigated as alkali-activated precursors and for soil stabilisation, to name a few, olivine[35–37], calcined clay[38], and pumicite[39–41].

In determining which precursor or combination of precursors to employ, it is crucial to consider practical factors such as local availability, material reactivity, and environmental impact. While precursors like fly ash, slag, palm oil fuel ash, or rice husk ash have proven successful in various regions, their availability and consistency of supply can be problematic in certain markets[42]. This challenge becomes more pronounced in countries that do not operate large coal-fired power plants, steel mills, or oil-processing industries on a sufficient scale, thereby limiting the consistent production of fly ash, GGBS, and palm oil fuel ash. In New Zealand, the transition towards renewable energy generation and low-emission, circular manufacturing practices has significantly reduced reliance on coal-fired power and traditional steelmaking[43–46]. As a result, the domestic production of industrial by-products such as fly ash and blast furnace slag has declined substantially. These limitations highlight the need to explore alternative precursors that are readily available and suitable for alkaline activation.

Approximately 130 million tonnes of Waste glass (WG) are generated globally each year, with less than 35% recycled[47,48]. Recycling WG involves several complex processes, including sorting, crushing, cleaning, and reprocessing[49]. These steps result in significant CO_2emissions, high costs, and considerable energy consumption. Consequently, reusing WG in the construction industry offers an efficient and environmentally beneficial solution to reduce its accumulation in landfills. Using reclaimed crushed glass in asphalt dates back to the 1970s[50]. The Australian Road Research Board's Best Practice guidelines recommend using recycled materials in road and rail infrastructure[51]. Reclaimed crushed glass is used in embankments, structural and non-structural fill, retaining wall backfill, and drainage. In these applications, glass particles help fill voids in the soil, resulting in a denser and more stable subgrade.

WG has also emerged as a noteworthy precursor in the context of alkali-activated binders[52,53]. Incorporating WG into alkali-activated systems can offer a twofold advantage: (i) it diverts substantial amounts of non-biodegradable glass from landfills, minimising environmental risks and disposal costs, and (ii) it leverages the silica-rich nature of glass to form robust aluminosilicate or alkali silicate reaction products[54,55]. In addition, prior research demonstrates that when properly ground or milled, WG can have comparable reactivity to traditional aluminosilicate materials, enabling sufficient strength development and reducing the carbon footprint associated with Portland cement production[56,57]. These features make WG a promising candidate for developing more sustainable soil stabilisation binders that address local waste management constraints and satisfy the performance requirements for subgrade improvement.

AAC has been using WG as a silicate activator[55,58], aggregate[59], and precursor[55,60]. Being rich in silica, WG is an ideal additive for the alkali-silica reaction in AAC[61]. Consequently, research has focused on modifying WG composition by incorporating Al- and Ca-rich materials, including red mud[62,63], metakaolin[55,64], fly ash[57,65], and ground granulated blast-furnace slag[66–69]. Additionally, AAC formulations using WG combinations with Portland cement[70,71], metakaolin and GGBS[64,72], or fly ash and ground granulated blast-furnace slag[56,73,74] have been explored. These mixtures, called binary and trinary precursors, further enhance the properties of AAC.

The literature indicates that optimal levels of partial replacement of WG with other aluminosilicate sources can enhance its performance in AAC. However, exceeding these optimal levels weakens mechanical strength due to the brittle nature of WG and the formation of high-volume alkalis[66,72]. Maldonado-Alameda et al.[75]developed alkali-activated binders using a combination of ceramic, stone, and porcelain waste, which included 84% soda-lime WG, combined with residues from the secondary aluminium production process as an Al-rich material. Additionally, replacing 35% of Portland cement with fluorescent lamp glass waste resulted in unconfined compressive strength (UCS) values comparable to Portland cement-based samples after 90 days of curing[76].

Glass has also been used as a trinary precursor in slag-fly ash-based AAC for pavement applications. A sample containing 15% glass achieved a compressive strength of 39.7 MPa after 7 days[77]. Several studies have investigated the efficacy of recycled glass powder-based geopolymers in stabilising clay soils. Burciaga-Díaz et al.[64] reported a significant increase in compressive strength by reaching approximately 35 MPa when using 30% WG as a partial replacement for metakaolin in their geopolymer recipe. Bilondi et al.[78] stabilised clayey soils using a recycled glass powder-calcium carbide residue-based geopolymer with glass content ranging from 0 to 9%, resulting in a nearly 60% improvement in compressive strength. Baldovino et al.[79] used a mixture of 5% hydrated lime and WG to stabilise silty soil, meeting all the requirements for earthworks applications after 90 days of curing. Más-López et al.[80] reported a compressive strength of 2.38 MPa for limestone stabilised with a pozzolanic binder containing 8% WG. Onitsuka, Shen[81] examined the effect of lime content on glass-based stabilised clay, finding that adding 20% lime content to WG contributes to compressive strengths ranging from 1.70 to 1.91 MPa. However, there is a research gap on the performance of WG as the sole precursor in

AAC because the chemical composition of WG significantly influences the properties of the produced cement, especially when it contains Ca^{2+} and Mg^{2+}phases like car windscreen WG which, according to Hamouda, Akhlaghi Amiri[82], facilitate the precipitation of sodium-silicate gels. This suggests that selective types of WG, particularly car windscreen WG, contain the necessary components for stable silicate gel formation, making it a promising sole precursor for glass-based alkali-activated cement (GBAAC).

This study introduces WG as the sole precursor in producing GBAAC in stabilising pumice sand, a loose soil in New Zealand. By utilising WG as an alternative precursor, this research aims to facilitate a higher recycling rate of this waste stream. The initial phase optimises the activator-to-precursor and unground-to-ground WG ratios for paste production. The UCS test was employed to assess the performance of the paste under varying curing temperatures and aging durations. Microstructural characteristics of the GBAAC will be analysed using Scanning Electron Microscopy (SEM) coupled with Energy-Dispersive X-Ray Spectrometry (EDS). In the second phase, the performance of GBAAC in stabilising pumice sand for road construction will be evaluated using the California Bearing Ratio (CBR) test.

This research represents a significant innovation in several key areas, including sustainability, infrastructure development, waste management, and soil stabilisation. It addresses critical challenges such as the environmental impact of Portland cement production[83], the unavailability of fly ash and slag[84], and the need for effective WG recycling. By successfully utilising WG to produce GBAAC for stabilising pumice sand, this study contributes to a more sustainable and environmentally friendly approach to construction.

Materials & methods

Materials

Pumice sand

The pumice sand used in this research was supplied by Daltons, a local manufacturer and supplier of landscape products in New Zealand. The obtained pumice sand, a by-product of their sand processing operation in Matamata that undergoes washing, screening, and grading to ensure its quality, was selected for its consistency, ensuring repeatability in the testing process. Two pumice sand products were initially selected for analysis, including a coarse (maximum particle size: 7 mm) and a fine (maximum particle size: 3 mm). The impact of compaction energy on the particle size distribution of both products revealed a more pronounced crushing effect on the pumice grains in the fine fraction than in the coarse fraction. Due to its lower sensitivity to compaction forces and more consistent behaviour, the coarse pumice sand (PS) exhibited greater suitability for comparative studies where the primary focus extends beyond purely mechanical stabilisation (Fig. 1a). Therefore, PS was selected for subsequent processes. Figure 2a shows a coarse pumice particle under SEM.

Particle size distribution analysis, conducted using a combination of sieve analysis[85] and hydrometer analysis[86] as illustrated in Fig. 3a, classified the PS as poorly graded sand (SP) according to the Unified Soil Classification System (USCS). Further Laser Particle Size Distribution (LPSD) analysis on the fine portion of the SP (particles smaller than 0.075 *mm*) was conducted using a Mastersizer 2000 Laser analyser revealing an average D50 of 33.99 μm (Fig. 3b). The Specific Surface Area (SSA) of particles smaller than 75 μm obtained from LPSD and Brunauer, Emmett and Teller (BET) analysis, measured from N_2 gas adsorption-desorption isotherms at the temperature of liquid nitrogen (−196 °C), are equal to 0.93 m^2/g and 9.03 m^2/g, respectively.

The compaction behaviour of pumice sand is significantly influenced by its lightweight, porous, and vesicular structure, which enables substantial water absorption and aids particle rearrangement during compaction[87]. Standard Proctor tests[88] indicated a distinctive double-peak compaction curve (Fig. 4) with maximum dry unit weights of 6.7 kN/m^3 (dry side) and 7.2 kN/m^3 (wet side), corresponding to optimum moisture contents of 10% and 40%, respectively. The initial densification at lower moisture (dry side) occurred primarily due to particle rearrangement and improved particle packing. At higher moisture content (wet side), the lubricating effect of water further reduced internal friction, enabling more efficient particle rearrangement and higher densities. Consequently, the optimum moisture content of the wet side (40%) was selected to achieve the maximum dry density.

Fig. 1. Images of the **(a)** coarse pumice sand (PS) and **(b)** glass powder (GP).

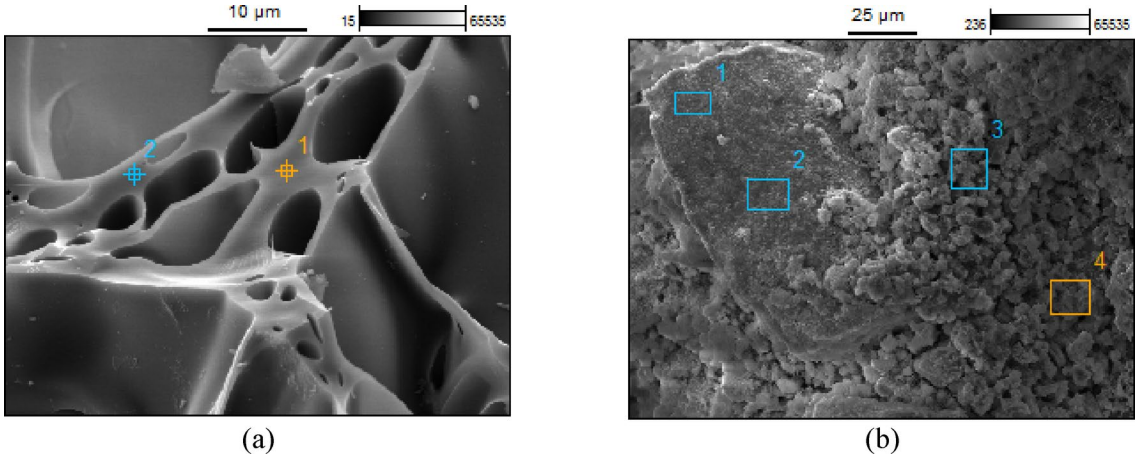

Fig. 2. SEM images of **(a)** coarse pumice sand (PS) and **(b)** glass powder (GP).

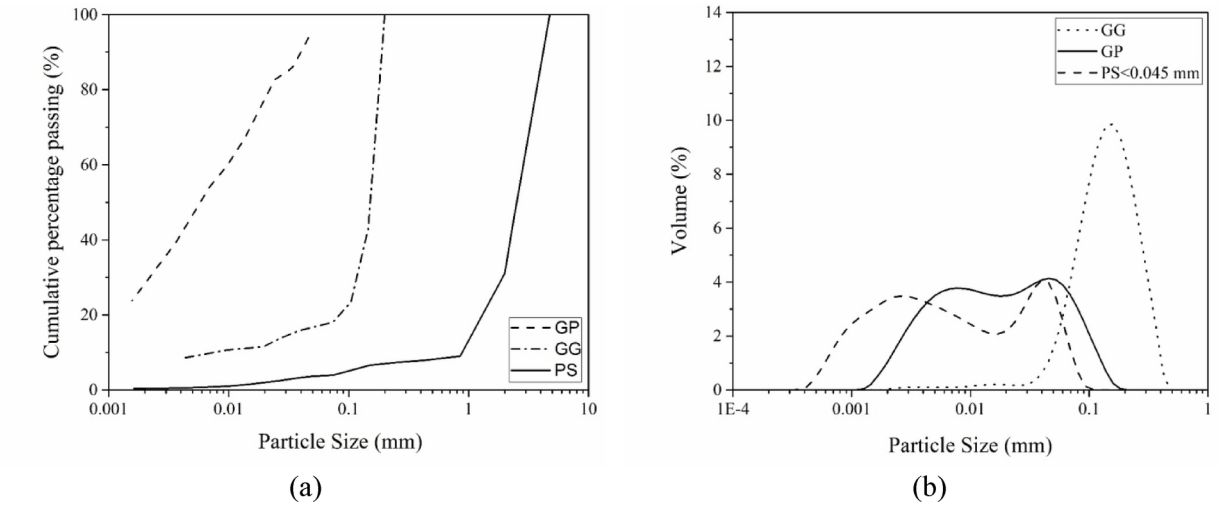

Fig. 3. Particle size distribution of the original coarse pumice sand (PS), glass powder (GP), and ground glass (GG) using **(a)** sieve analysis and **(b)** Laser Particle Size Distribution (LPSD).

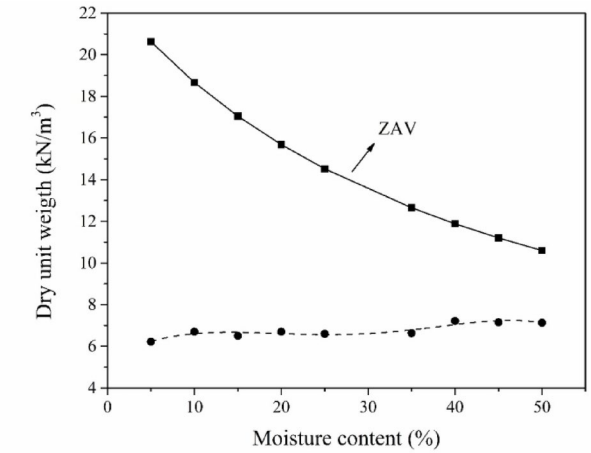

Fig. 4. Compaction curve of the coarse pumice sand (PS).

Material	Chemical Components (Weight%)								
	SiO_2	Al_2O_3	Fe_2O_3	CaO	MgO	Na_2O	K_2O	TiO_2	LOI
PS	74.0	14.0	1.0	1.3	0.3	3.0	4.0	0.1	~ 2.3
GP	72.0	< 0.08	< 0.05	< 9.50	< 6.00	< 15.00	< 0.03	-	-

Table 1. Chemical elements of the PS and GP obtained from XRF analysis.

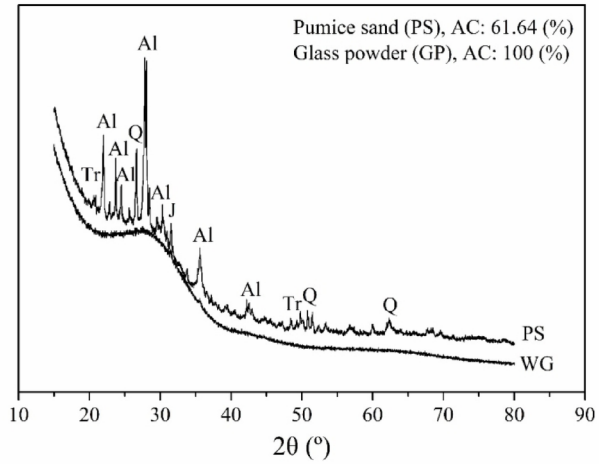

[Q: quartz, Al: albite, Tr: tridymite, J: Jadeite]

Fig. 5. XRD results for coarse pumice sand (PS) and glass powder (GP).

Table 1; Fig. 5 present X-ray fluorescence (XRF) and X-ray Diffraction (XRD) results to determine the chemical element and mineralogy of the materials, respectively. The XRF results for PS show SiO_2 with 74% by weight as the main chemical component followed by 14% Al_2O_3. The remaining components comprise less than 10% by weight of the PS, and around 2.3% is loss on ignition (LOI) during the test. The XRD pattern, measured with a PANalytical Empyrean diffractometer equipped with Cu Kα-ray source and PIXcel 1D, illustrates the presence of aluminosilicate minerals including albite ($NaAlSi_3O_8$, 90.8%), tridymite (SiO_2, 4.3%), quartz (SiO_2, 3.0%) and Jadeite ($NaAlSi_2O_6$, 1.8%). These minerals comprise 38.35% of the total phase, indicating the remaining 61.64% as the amorphous phase.

Waste glass

The waste glass powder (GP), sourced from Commodities NZ Ltd. in 25 kg bags, is a powder product of car windscreen glass with particles under 0.2 *mm*, in the fine sand range (Fig. 1b). Figure 2b shows the morphology of GP, which exhibits an irregular, angular morphology attributed to the milling processes in the recycling facility. The particle size distribution of GP was determined using two methods, the hydrometer analysis shown in Fig. 3a, and the LPSD illustrated in Fig. 3b. With a D_{50} = 133.04 μm, the GP is mainly in the range of fine sand with around 15–20% silt content. The GP exhibits very low plasticity and is classified as poorly graded sand (SP) based on the USCS. Its SSA and BET surface area equal 0.029 m^2/g and 0.495 m^2/g, respectively. The XRF results in Table 1, show SiO_2 as the most abundant component with 72% by weight of GP, followed by 15% NaO_2, 9.5% CaO, and 6% MgO. Traces of aluminium, iron, and potassium oxides are detected with less than 0.1% by weight of the GP.

The XRD pattern in Fig. 5 reveals a 100% amorphous phase in GP, with no detectable mineral phases. The amorphous silica in GP can be reactive. Mechanical treatment was employed to enhance GP reactivity by producing finer glass particles. A Retsch planetary ball mill (PM 100 CM) was used for grinding, with 16 stainless steel balls (15 mm diameter) and a rotating speed of 600 RPM. Varied grinding parameters were examined (5, 10, 15, 20, and 40 min) and the optimal grinding performance was achieved with a half-loaded jar and a grinding duration of 20 min. Hydrometer analysis (Fig. 3a) and LPSD analysis (Fig. 3b) demonstrated a significant shift in the particle size distribution towards smaller particles after grinding. The optimised ground glass (GG) exhibited significantly finer particles, with D10, D50, and D90 values of 3.495 μm, 17.978 μm, and 72.722 μm, respectively, compared to 61.847 μm, 133.315 μm, and 255.572 μm measured for the GP. Approximately 30% of GG particles fell within the targeted size range (< 100 μm). The increase in SSA to 0.28 m^2/g further confirmed the enhanced reactivity of the GG.

Alkaline activator

A 10 M KOH solution was used as an alkaline activator. KOH pellets with a specific gravity of 2.04 at 20 °C (88 wt%), supplied by ThermoFisher Scientific New Zealand, were used. To prepare the alkaline solution, KOH pellets were slowly added to distilled water in a beaker placed on an ice bath within a chemical hood. The mixture was stirred continuously until the pellets were completely dissolved. The solution was then allowed to cool to room temperature for at least 48 h before use.

Experimental programme

Figure 6 illustrated the experimental programme of the study, including material preparation, samples preparation, and test plan.

Sample preparation

Details of the specimens synthesised for this research are included in Table 2. The experiment involved three groups. Group I aimed to optimise GBAAC by investigating the influence of the activator-to-precursor ratio (A/*P*= 0.1 to 0.5) on compressive strength according to[89]. Based on the optimal A/P ratio determined in Group I experiments, Group II specimens were designed to investigate the influence of particle size distribution of precursor (GP/GG = 1, 1.5, and 2.33) on the compressive strength of the paste. The dry mix of GP and GG (GPG) for Group II was prepared using a mechanical mixer. Determining the optimal GP/GG ratio minimises grinding time and energy consumption while maintaining sufficient reactivity and strength development. Three identical samples were prepared for each mixture in both groups, and average values were reported.

Group III specimens were designed based on the optimised results of Group II to investigate the effect of WG on the bearing capacity of PS, both as non-activated fine aggregates and as activated GBAAC, using the CBR tests. To ensure the reliability of the results, two identical samples of each mix design in Group III were initially prepared and tested. If the results did not meet the accuracy and precision requirements specified in the CBR testing procedure, additional samples were prepared and tested until the criteria were satisfied.

To make the specimens in groups I and II, GG and GPG were mixed with the alkaline activators, respectively, according to the ratios described in Table 2. Materials were mixed for 10 min using a mechanical mixer with occasional hand mixing. The fresh paste was then placed into standard cubical steel moulds of 50 mm in three equal layers. Each layer was compacted using a vibration desk operated at 3500 vibrations per minute to expel air bubbles from the samples. Samples were cured at 65 °C for 48 h, then demoulded and stored at room temperature for 24 h before testing. Additional samples of the optimised mix were made with different curing and aging conditions for further study.

Group III samples were prepared and tested according to the standard test procedures for both standard (3-layer light compaction) and modified (5-layer heavy compaction) CBR tests[88,90,91]. The key steps included

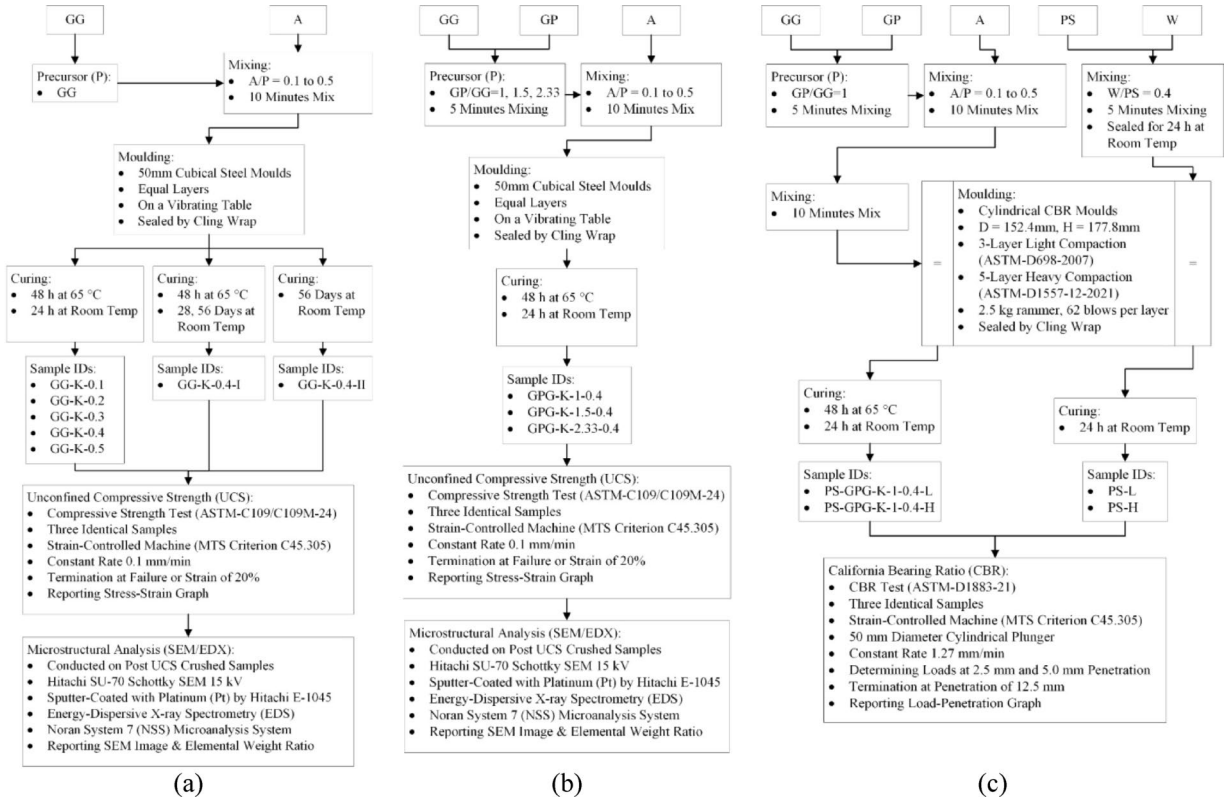

Fig. 6. Testing process flowchart for **(a)** Group I, **(b)** Group II, and **(c)** Group III.

Group	Sample ID	A/*P* (%)	K (Molar)	GP/GG (%)	*P*/PS	Test	Curing Condition	RT Aging (day)
I	GG-K-0.1	0.1	10	-	-	UCS	ET	1
	GG-K-0.2	0.2	10	-	-	UCS	ET	1
	GG-K-0.3	0.3	10	-	-	UCS	ET	1
	GG-K-0.4	0.4	10	-	-	UCS	ET	1
	GG-K-0.5	0.5	10	-	-	UCS	ET	1
	GG-K-0.4-I	0.4	10	-	-	UCS	ET	28, 56
	GG-K-0.4-II	0.4	10	-	-	UCS	RT	56
II	GPG-K-1-0.4	0.4	10	1	-	UCS	ET	1
	GPG-K-1.5-0.4	0.4	10	1.5	-	UCS	ET	1
	GPG-K-2.33-0.4	0.4	10	2.33	-	UCS	ET	1
III	PS-L	-	-	-	-	S-CBR	RT	1
	PS-H	-	-	-	-	M-CBR	RT	1
	PS-GPG-K-1-0.4-L	0.4	10	1	0.3	S-CBR	ET	1
	PS-GPG-K-1-0.4-H	0.4	10	1	0.3	M-CBR	ET	1

Table 2. Mixture proportions and details of the experimental programme. Notes: A/P = Activator to Precursor Ratio; K = 10 M KOH Solution; GG = Ground Glass; GP = Glass Powder; P = Precursor; PS = Pumice Sand; RT = Room Temperature; ET = Elevated Temperature (65°C) for 48 h; L = Three-Layer Compacted Standard CBR (S-CBR); H = Five-Layer Compacted Modified CBR (M-CBR); GPG = GG-GP Mix. The mixture proportions included in the table can be calculated as follows: • Group I: The activator weight is determined by multiplying the A/P ratio by the given precursor weight. • Group II: The precursor is a combination of GP and GG. The required weight of GP is obtained by multiplying the GP/GG ratio by the given GG weight. The total weight of GG and GP is considered the precursor weight. The activator weight is then calculated by multiplying the A/P ratio by the total precursor weight. • Group III: PS-L and PS-H do not contain any precursor or activator. For the other two samples, the required precursor weight is determined by multiplying the P/PS ratio by the given PS weight. A unit ratio of GG/GP is then used to prepare the required precursor. Finally, the activator weight is calculated by multiplying the A/P ratio by the precursor weight.

material preparation based on the optimised GBAAC with ratios outlined in Table 2, followed by compaction in the CBR mould moulds with a diameter of 152.4 mm and a height of 177.8 mm using a standard 2.5 kg rammer with 62 blows per layer. The GBAAC-stabilised PS samples were cured at 65 °C for 48 h. All samples in this group were sealed and stored at room temperature for 24 h before testing.

Two subgroups of samples were prepared: mechanically stabilised PS and mechano-chemically stabilised PS with the addition of the optimised GBAAC. This allowed for investigation of the binder's impact on the stabilised soil's performance. Recent research on soil stabilisation indicates a wide range of AAC binder additions (20–30% by dry weight of soil), with the specific percentage varying based on soil type and desired strength[92,93]. Given the non-cohesive nature of PS, 30% GPG by weight of the dry soil was used as the precursor content for the required amount of the GBAAC to be used as a stabilisation agent in this study.

Due to its high porosity, PS exhibits high moisture absorption capacity, with a surface dry moisture content of approximately 40%. This coincides with the optimum moisture content of PS determined from the standard Proctor test. Bringing the PS moisture content to its surface dry level enhances the workability of the mixture, prevents dilution of the alkaline solution and maintains the necessary moisture content for the alkali activation process. Therefore, 40% water content by weight was mixed with the PS for 5 min using a mechanical mixer and left in a sealed bucket at room temperature for 24 h before sample preparation to homogeneous moisture.

Compressive strength test

The compressive strength test[89] was conducted on three identical specimens from each mixture recipe in groups I and II. The tests were performed on the prepared cubic specimens with a loading rate of 0.1 mm/min using a strain-controlled Universal Testing Machine (UTM), specifically an MTS Criterion C45.305 with a 300 kN capacity. The termination criteria were defined as either failure of the specimen or reaching a maximum strain of 20%. Stress-strain curves were generated for each specimen, and the maximum compressive strength was determined. The average of the three test results for each mixture was reported.

CBR test

The CBR test, a standard method for pavement design and road construction, was employed to evaluate the strength characteristics and load-bearing capacity of the samples in group III. This group of samples was designed to investigate the influence of various factors on the load-bearing capacity of PS mixtures, including the inclusion of WG (both as fine aggregate and as GBAAC), the particle size distribution of PS, and compaction effort (light and heavy compaction methods).

CBR testing was conducted by driving a 50 mm diameter cylindrical penetration plunger into the top surface of the specimen at a constant rate of 1.27 mm/min, with the load applied using the UTM device. Load and

penetration resistance were recorded continuously to determine the loads at 2.5 mm and 5.0 mm penetration depths, which were then compared to standard load values to calculate the CBR percentage. Additionally, the ultimate performance of each sample was measured at 12.5 mm penetration.

Microstructural analysis

SEM/EDX analysis was conducted using a Hitachi SU-70 Schottky field emission scanning electron microscope at an accelerating voltage of 15 kV. SEM/EDX analysis was performed on the crushed samples after the compressive strength test. The crushed samples were sputter-coated with Platinum (Pt) for 100 s using a Hitachi E-1045 ion sputter coater to improve electrical conductivity. The elemental composition of the samples was determined using EDS with a Noran System 7 (NSS) microanalysis system.

Results and discussion

Glass-based alkali-activated cement

Group I UCS results

Figure 7a shows the stress-strain curves of the Group I specimens after 48 h of curing at 65 °C, followed by 24 h of room-temperature curing. Specimens GG-K-0.1 and GG-K-0.2 exhibited relatively ductile behaviour, failing at low stress and strain levels (approximately 0.02–0.25). In contrast, GG-K-0.3, GG-K-0.4, and GG-K-0.5 demonstrated stiff behaviour with an initial linear-elastic region followed by a more gradual decline in stress (strain softening) before failure, reaching failure at higher strains (between 0.04 and 0.05) and achieving higher peak stresses. Furthermore, these specimens demonstrated a higher initial modulus of elasticity, as evidenced by the steeper initial slopes of their stress-strain curves.

It is evident that pastes with a lower A/P ratio, i.e., GG-K-0.1 and GG-K-0.2, tended to exhibit more plastic behaviour before and after their peak strength. In contrast, pastes with a higher A/P ratio, i.e., GG-K-0.3, GG-K-0.4, and GG-K-0.5, exhibited a more brittle behaviour, showing a clear peak strength followed by a sharp decline in stress during excessive deformation, similar to observations made by Pourakbar et al.[94]. This suggests that higher A/P ratios effectively promoted the alkaline activation process of the WG.

The compressive strength of the paste increased significantly from 4.8 MPa to 36.9 MPa as the A/P ratio increased from 0.2 to 0.3. However, further increases in the A/P ratio, from 0.3 to 0.4 and then to 0.5, resulted in only minor changes in UCS, with values remaining relatively stable (Fig. 7b). Specifically, GG-K-0.3 and GG-K-0.5 exhibited similar UCS values (36.9 MPa and 36.5 MPa, respectively). In comparison, GG-K-0.4 achieved the highest UCS of 37.9 MPa. Therefore, the A/P ratio of 0.4 was selected as the optimum. This finding is consistent with research by Redden, Neithalath[54] and Samarakoon et al.[56], who also identified an A/P ratio of 0.40 optimal for producing glass-based geopolymer with the highest early strength. Furthermore, Redden, Neithalath[54] reported UCS values of approximately 32 MPa for WG activated by 8 M NaOH, cured at 75 °C for 24 h, which is comparable to the results of this study.

This observation highlights the significant influence of the A/P ratio on the development of alkaline activation. An optimal amount of activator is necessary to initiate the dissolution of solid particles, progressing from the outside inward through an alkaline attack[95], and to facilitate the mobility of the dissolved phases[94,96]. However, an excessive A/P ratio can lead to a lower degree of binding product formation and increased porosity, consequently reducing compressive strength[97]. This excess can also slow the dissolution and mobility of aluminosilicate phases due to increased free water and electrostatic shielding[96,98]. Therefore, a 10% increase in the A/P ratio from 0.2 to 0.3 significantly improved alkaline activation and binding formation compared to the further increase from 0.4 to 0.5, which negatively affected compressive strength due to increased residual water and the formation of small pores.

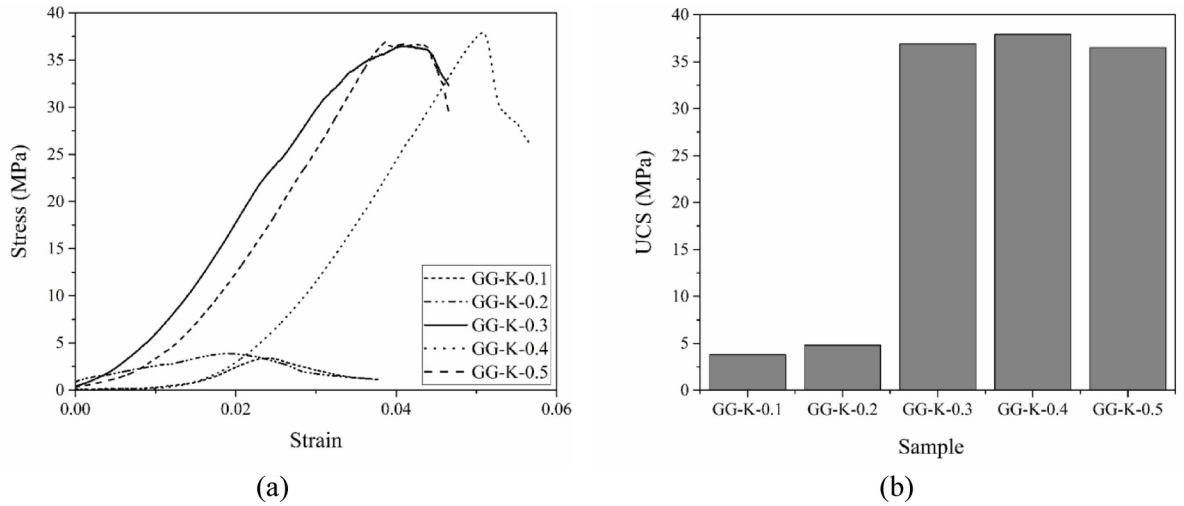

Fig. 7. **(a)** Stress-strain behaviour, and **(b)** UCS values of the samples defined in group I.

Figure 8a shows the variation in UCS values of GG-K-0.4 and GG-K-0.4-I with increasing aging times. Increased aging from 3 to 28 days decreased UCS from 37.9 to 24.5 MPa, followed by a substantial increase to 65 MPa after 56 days. This increase in strength with extended aging (56 days) can be attributed to enhanced precursor dissolution and the formation of binding gels. The initial decrease in UCS at 28 days may be due to silica depolymerisation within the alkali gels under ambient humidity. Subsequently, the increasing alkalinity promotes further alkaline reactions and gel production, eventually overcoming the initial depolymerisation. This suggests that the prolonged curing time at 56 days allowed polymerisation to surpass depolymerisation. This trend is consistent with Redden, Neithalath[54], who observed a sharp decrease in UCS after 7 days of moist curing, followed by a further reduction after 28 days, compared to heat-cured samples (24 h at 75 °C) of WG activated by 8 M NaOH solution.

As shown in Fig. 8b, elevated curing temperature significantly influences the alkaline activation of glass after 56 days of aging. GG-K-0.4-II samples, cured at 65 °C for 48 h, achieved a UCS of 65 MPa, which is 2.6 times higher than the average UCS of 25.3 MPa achieved by GG-K-0.4-RT samples cured at room temperature after 56 days. However, a strength of 25.3 MPa is still practical for soil stabilisation applications. This substantial difference demonstrates the significant effect of high temperature on binding gel formation compared to the slower reaction kinetics of WG at room temperature. Elevated temperatures promote residual water evaporation and increase matrix alkalinity, accelerating alkaline reactions. Conversely, at room temperature, precursor dissolution and condensation processes are slowed[99]. Overall, increased aging time and elevated curing temperature enhance the interaction between the alkaline activator and the precursor in dissolution and condensation processes[100–102].

Except for GG-K-0.1 and GG-K-0.2, all other UCS values in Group I are significantly higher than the 9 MPa reported by Cristelo et al.[103] for samples composed of 100% precursor WG. This difference in strength may be attributed, at least in part, to differences in the chemical composition of the glass. The WG used by Cristelo et al.[103] contained 6.12% CaO and 3.94% Al_2O_3. While a lower Al_2O_3 content (0.08%) is found in the WG used in this study, it has a higher CaO content (9.5%) and an additional 6% MgO, which can contribute to the alkaline reaction and subsequent strength gain[104,105].

Group II UCS results

Figure 9a shows how variations in the precursor particle size distribution (GP/GG ratio) affect the stress-strain behaviour of pastes prepared in Group II with a constant A/P ratio of 0.4. Increasing the GP/GG ratio (from 1 to 2.33) resulted in more plastic behaviour and a gradual reduction in both maximum strength and strain at peak stress. A less pronounced drop in post-peak mobilised stress was observed with increasing GP/GG ratio. This change in stress-strain behaviour corresponded to a decrease in UCS values from 19.3 MPa (GPG-K-1-0.4) to 11.4 MPa (GPG-K-1.5-0.4) and further to 4.3 MPa (GPG-K-2.33-0.4). The higher UCS values observed in specimens with a higher proportion of finer GG particles compared to coarser GP particles demonstrate the effectiveness of finer particle size distributions in promoting alkaline activation and the formation of binding gels (Fig. 9b). This aligns with the well-known principle that finer particles possess a higher SSA and reactivity, leading to increased release of Si, Ca^{2+}, and Mg^{2+} ions, and greater formation of binding gels during alkaline activation. Furthermore, the crushing process can introduce micro-cracks that weaken larger glass particles than finer particles. This explains why incorporating a greater proportion of larger particles reduced the UCS values, which aligns with observations by Samarakoon et al.[56]that finer WG particles enhance the formation of binding products and promote the agglomeration of unreacted glass powder. In addition, a higher proportion of fine particles improves particle packing and enhances density[106].

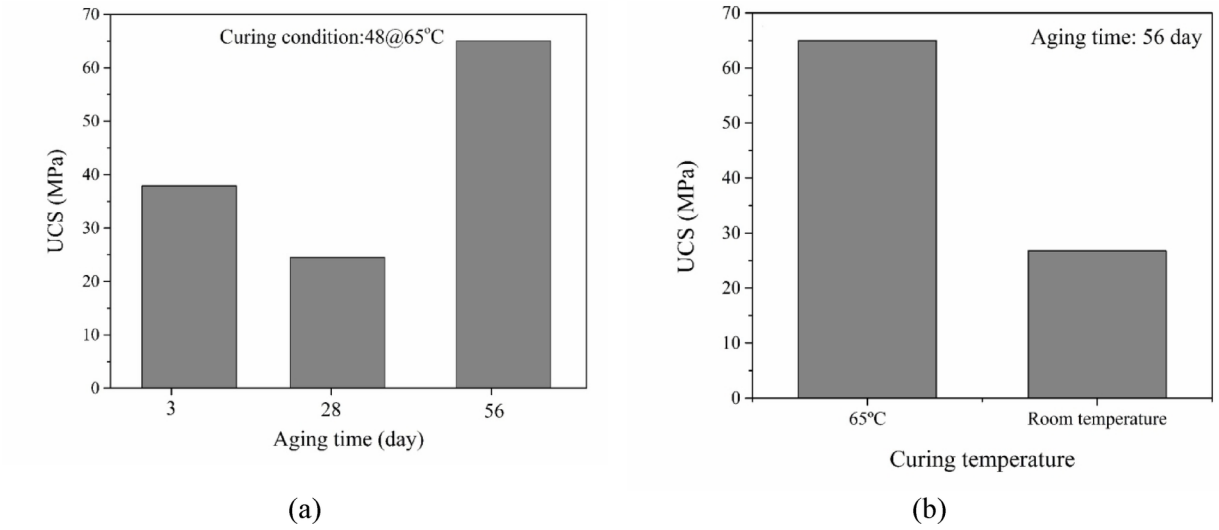

Fig. 8. Variations in UCS with **(a)** aging time for GG-K-0.4 vs. GG-K-0.4-I and **(b)** curing temperature for GG-K-0.4-I vs. GG-K-0.4-II.

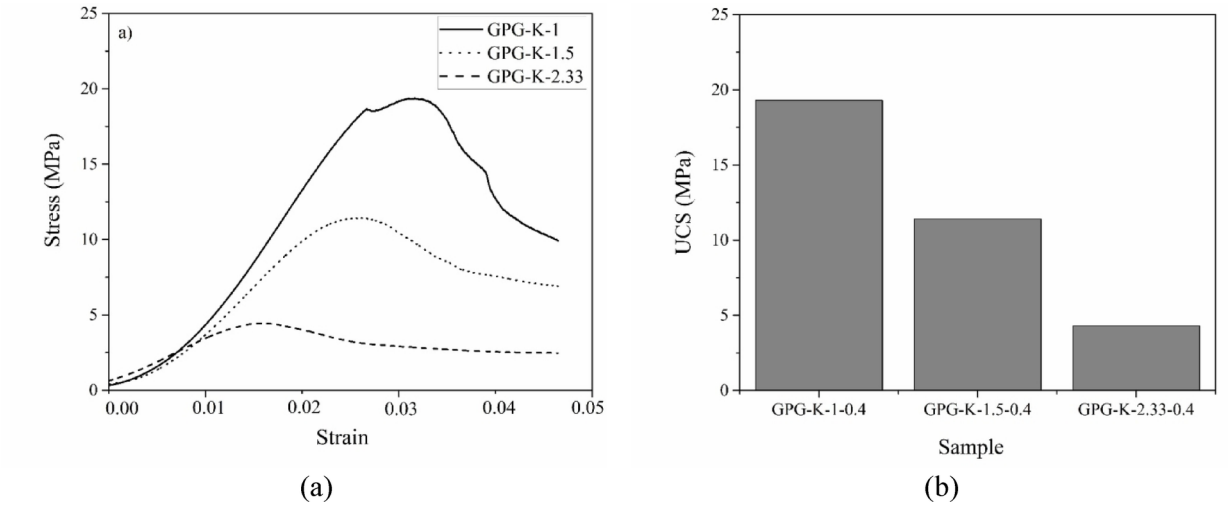

Fig. 9. **(a)** Stress-strain behaviour, **(b)** UCS values of the samples defined in group II.

The UCS of 19.3 MPa is considered moderate strength and is suitable for soil stabilisation, providing sufficient strength improvement without excessive stiffening of the subgrade upon careful design. In addition, a GP/GG ratio of one reduces the post-processing (grinding) of the GP by half, resulting in a 50% reduction in the energy and time required for precursor preparation, thereby significantly reducing the embodied time and energy of AAC. Therefore, GPG-K-1-0.4 is selected as the optimum paste mixture for the subsequent stage, where the GBAAC is used as a binder for stabilising PS.

Group I SEM/EDX analyses

Figure 10 presents the SEM/EDX results showing the microstructural characteristics of selected pastes from group I with different A/P ratios, including GG-K-0.1 (activator deficient), GG-K-0.4 (optimal activator level), and GG-K-0.5 (high activator content). The morphology of GG-K-0.1 (Fig. 10a) reveals agglomerated particles with unreacted WG and high porosity, resulting in a poorly connected microstructure. This indicates that the low activator content (A/*P*= 0.1) restricted glass dissolution and activation of the glass particles, leading to a weaker and less uniform microstructure, which is consistent with the low UCS (4.8 MPa).

Figure 10b and c show the morphology of GG-K-0.4 and GG-K-0.5, respectively, exhibiting homogeneous surfaces and well-bonded particles. However, the high activator content in GG-K-0.5 (A/*P*= 0.5) resulted in smoother, glossier surfaces, while the optimal activator content in GG-K-0.4 (A/*P*= 0.4) promoted improved flocculated particle formation. These intrinsically smooth, glossy surfaces have been shown to reduce UCS values by decreasing inter-particle friction[56], which correlates well with the observed UCS results: GG-K-0.4 (37.9 MPa) exhibited a higher UCS than GG-K-0.5 (36.5 MPa). The higher alkali content in GG-K-0.5 likely increased the number of non-bridging oxygen sites, altering the connectivity of the SiO_4tetrahedral network to silicate chains, dimers, and monomers, compared to GG-K-0.4, where the optimal alkali content likely reduced non-bridging oxygen sites in the silicate 3D frameworks and sheets. The micro-cracks evident in both specimens are attributed to shrinkage cracking caused by gel formation during heat curing[54].

EDX analysis revealed a very low alumina content in the glass powder, which is consistent with the XRF analysis of GP (Al_2O_3< 0.08) and likely hindered the formation of N-A-S-H gels. However, the incorporation of Ca and Mg is also evident within the produced gels. In GG-K-0.1 (Fig. 10a), Na was the primary element involved in the formation of the initial gels, followed by Ca, Mg, and K, suggesting the predominant formation of alkali silicate gels. In GG-K-0.4 and GG-K-0.5, the predominant involvement of Na and K, followed by Ca and Mg, suggests the dominant formation of alkali/alkaline-earth-silicate-hydrate gels (C/Mg-N/K-S-H). Dissolved Si-O^- ions primarily react with Na^+ and K^+ to form silicate gels. A smaller proportion of Si-O^- ions may also react with Ca^{2+} and Mg^{2+} to generate C/Mg-N/K-S-H gels.

A key observation from the comparison of GG-K-0.4 and GG-K-0.5 is that the former exhibited a lower Na/Si ratio and a higher Mg/Si ratio. This suggests a greater incorporation of Mg and a lesser incorporation of Na into the binding gels, which is beneficial because it promotes the formation of alkali silicate gels with stronger intermolecular bonds and increased hardness. Divalent cations such as Mg^{2+} and Ca^{2+}, with their greater electrical field strength compared to monovalent alkali ions such as Na^+ and K^+, exert a stronger influence on the bond strength within the silicate network[107]. Furthermore, the lower mobility of Mg^{2+} and Ca^{2+} compared to Na^+ and K^+ can restrict alkali diffusion[106]. Consistent with these observations, it is well established that high Na_2O/SiO_2 ratios are associated with inferior mechanical properties[107], which explains why GG-K-0.4, with its lower Na/Si ratio, exhibited the maximum UCS value.

The effect of prolonged aging time on the microstructural characteristics of the optimised paste was done by SEM/EDX analyses on GG-K-0.4-I and GG-K-0.4-II samples. Different morphologies are evident in specimens cured at different temperatures. Point 3 in Fig. 11a depicts the presence of Zeolite in the GG-K-0.4-I sample initially cured at 65°C for 48 h before the 56 days aging process starts at room temperature. The Ca/Si ratio of

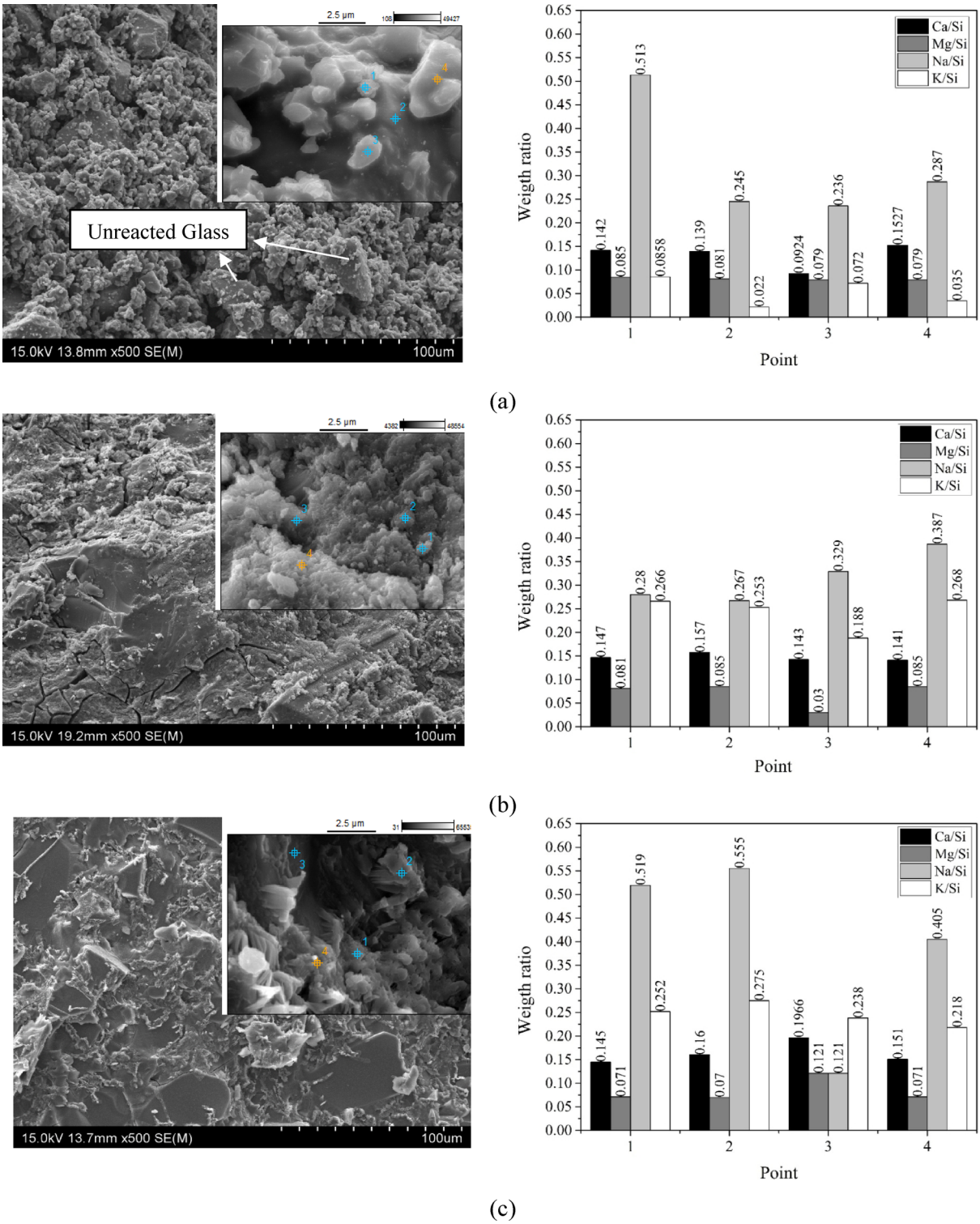

Fig. 10. SEM/EXD results of **(a)** GG-K-0.1, **(b)** GG-K-0.4, **(c)** GG-K-0.5.

the aged sample is higher than the young sample (GG-K-0.4 in Fig. 10b), while Mg/Si has showed a little loss (points 1 and 4 in Fig. 11a). That is an indication of adsorption of more Ca^{2+} and less Mg^{2+}in binding gels due to the prolonged aging time. In general, the low Ca/Si molar ratio results in the production of sodium silicate gel prone to depolymerisation, while the rise in this ratio produces more of the strong bonds. Hamouda, Akhlaghi Amiri[82] found that the presence of Ca^{2+} and Mg^{2+} ions increase the strength of alkaline sodium silicate gels which explains the enhanced strength for the 56-day-aged sample. Figure 11b refers to the higher Na/Si and K/Si ratios for GG-K-0.4-II compared to the sample cured at elevated temperature (GG-K-0.4-I). This means curing at high temperature restricted the participation of alkalis, i.e., Na^{+} and K^{+}, into the reaction products which is

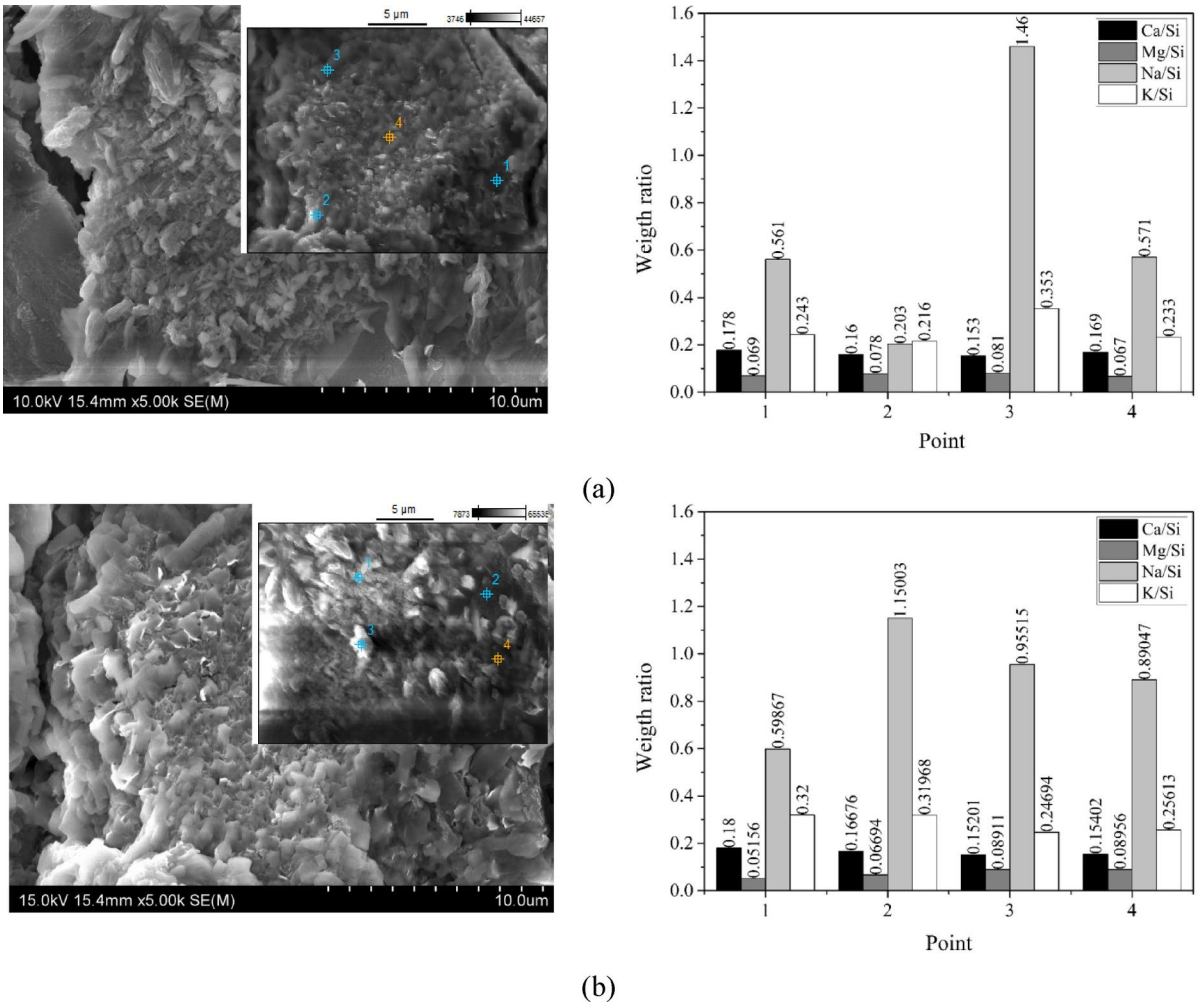

Fig. 11. SEM/EDX analysis of 56-day aged samples: **(a)** GG-K-0.4-I and **(b)** GG-K-0.4-II.

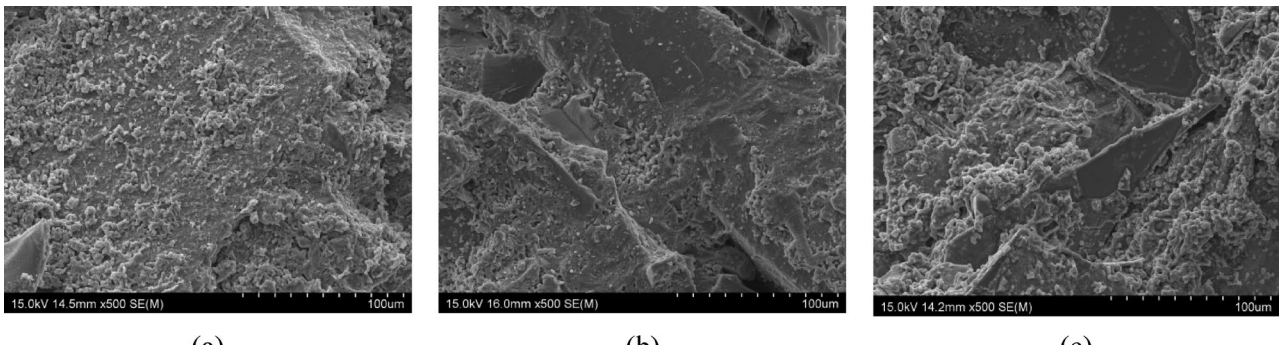

Fig. 12. SEM results of samples prepared in of Group II with GP/GG = 1, 1.4 and 2.33, **(a)** GPG-K-1-0.4, **(b)** GPG-K-1.5-0.4, and **(c)** GPG-K-2.33-0.4.

another reason for higher final UCS for GG-K-0.4-I (65 MPa) compared with GG-K-0.4-II (25.3 MPa) after the 56-day aging.

Group II SEM analyses

Figure 12 presents the SEM results of Group II specimens with three different GP/GG ratio presented in Table 2 to show how variations in the precursor particle size distribution (GP/GG ratio) affect the stress-strain behaviour of the pastes. Figure 12a shows GPG-K-1-0.4 exhibiting a homogeneous morphology. In contrast, Fig. 12b and c,

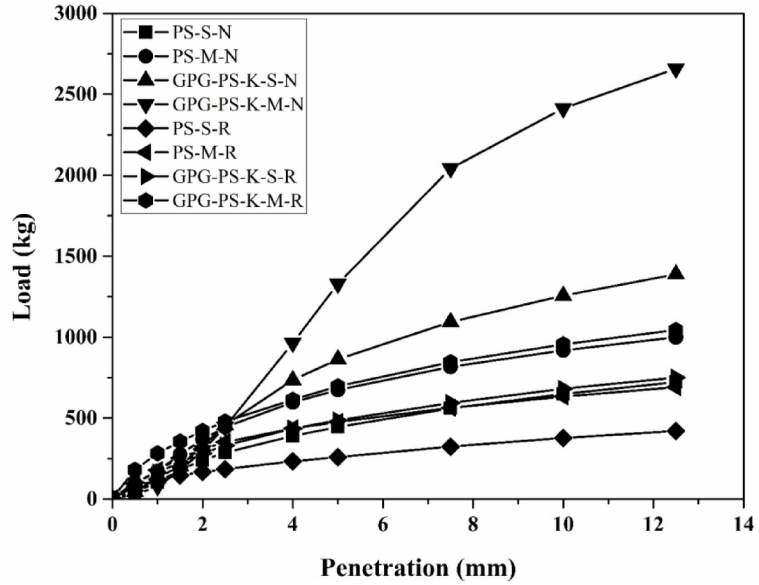

Fig. 13. CBR results for the stabilised PS.

Mixture ID	Avg. $CBR_{2.5}$(%)	Avg. $CBR_{5.0}$(%)
PS-L	20.88	21.64
PS-H	32.41	32.79
PS-GPG-K-1-0.4-L	33.35	41.98
PS-GPG-K-1-0.4-H	32.50	64.70

Table 3. CBR test results for stabilised pumice soils defined in group III.

depicting GPG-K-1.5-0.4 and GPG-K-2.33-0.4, respectively, clearly show unreacted WG particles. Specifically, Fig. 12c reveals a dispersed morphology with a greater amount of unreacted glass visible as the GP content increases. Consistent with the UCS results discussed earlier, the SEM observations indicate that a higher GP/GG ratio limits precursor reactivity and reduces the formation of alkali-activated gels. The increased inclusion of GP, particularly larger particles, leads to a reduced alkaline reaction, limiting interconnections and resulting in a less compact microstructure.

Stabilised pumice sand

CBR test results

The CBR test is a widely used laboratory method for evaluating the relative strength of a soil sample by comparing its resistance to penetration with that of a standard material, typically crushed stone or well-graded aggregate. This test provides valuable information regarding the soil's capacity to withstand applied loads and suitability for various pavement construction applications. Multiple samples were carefully prepared and tested according to the standardised CBR test procedure to investigate the strength characteristics of pumice soil stabilised with the GBAAC.

Initially, two samples of each mix design were prepared and tested to assess the accuracy of the results. Additional tests were performed in some cases to ensure the required precision. Figure 13 shows CBR graphs regarding load versus penetration for all samples defined in group III. The consistent stress-strain behaviour observed across all sample pairs throughout the penetration range confirms the reliability of the results. Among the various mixes, the PS-GPG-K-1-0.4-H samples exhibited the highest ultimate strength, while the PS-L samples showed the lowest.

The CBR values presented in Table 3 are the averages of two samples with acceptable accuracy for each mix design. These values reflect the load-bearing capacity of the tested soil samples; higher CBR values indicate greater strength and load-bearing capacity. Among the tested mix designs, PS-L underperformed at lower penetration levels than the other three samples, exhibiting relatively similar performance. At higher penetration levels, a consistent and gradual increase in strength was observed from PS-L to PS-H and then to PS-GPG-K-1-0.4-L. While both GBAAC-stabilised samples outperformed PS-L and PS-H, PS-GPG-K-1-0.4-H demonstrated superior performance at higher penetration levels, likely due to the heavy compaction, facilitating optimal binding between the AAC and pumice sand particles. This mixture showed strong resistance to penetration and high load-bearing capacity, indicating its suitability for heavy load applications.

These results allow for interpretation regarding the impact of several parameters on the strength gain of the stabilised PS. The first parameter is the effect of compaction on soil strength, where samples subjected to higher compaction efforts using 5-layer compaction exhibit greater strength than those prepared using 3-layer compaction. Relevant graphs can also be compared to examine the role of the GBAAC in stabilising pumice soil. Across all samples, the CBR graphs demonstrate superior strength gain in samples stabilised using the GBAAC, providing evidence of the effectiveness of this binder for stabilising pumice sand in road subgrades. Although the graph indicates that the best-performing pairs, PS-GPG-K-1-0.4-L and PS-GPG-K-1-0.4-H, are those stabilised using the AAC, further analysis can enhance our understanding of the relatively good performance of the mechanically stabilised samples (PS-H) at lower penetration levels up to 2.5 mm. While these results confirm the project's objectives, they also open the door for further investigation, research, and potential application of the proposed process in road construction.

Conclusions

This study developed a glass-based alkali-activated cement (GBAAC) for stabilising New Zealand pumice sand, enhancing its suitability as a subgrade material for road construction. The optimal mixture was achieved at an activator-to-precursor ratio of 0.4, cured at 65 °C for 48 h, resulting in a compressive strength of 37.9 MPa. This ratio enhanced particle flocculation and phase mobility, while activator deficiency or excess reduced strength due to incomplete dissolution or increased porosity. Strength initially decreased at 28 days due to depolymerisation but significantly improved at 56 days due to enhanced precursor dissolution, with elevated temperature curing producing 2.6 times higher strength than room temperature curing.

Microstructural analyses indicated the involvement of Na^+ and K^+, followed by Ca^{2+} and Mg^{2+}, confirming the formation of alkali and alkaline-earth silicate hydrate gels. The optimised particle size distribution of WG, consisting of equal proportions of unground and ground particles, offered sufficient compressive strength for soil stabilisation while reducing the energy and time required for material preparation.

CBR tests demonstrated substantial improvement in the strength and load-bearing capacity of pumice sand stabilised with GBAAC. The highest average CBR5.0 value of 64.70% was obtained when heavy compaction was combined with the optimised GBAAC binder, significantly exceeding the 21.67% observed in untreated, lightly compacted pumice sand.

While this study demonstrated that room temperature-cured samples achieved sufficient compressive strength for practical field applications, further research is recommended to evaluate the long-term durability, microstructural evolution, and field performance of ambient-cured GBAAC-stabilised pumice sand. Additional testing and analysis are also needed to understand the complex stress-strain behaviour observed at lower penetration levels, particularly the relatively strong performance of mechanically stabilised pumice samples (PS-H) at penetration depths up to 2.5 mm.

Data availability

All data generated or analysed during this study are included in this published article.

Received: 3 January 2025; Accepted: 16 April 2025
Published online: 01 July 2025

References

1. Gill, O. M. & Orense, R. P. Field characterisation and mapping of pumiceous deposits in central North Island, NZ. *Japanese Geotech. Soc. Special Publ.* **6**(2), 79–87 (2019).
2. Selby, M. & Hosking, P. The erodibility of pumice soils of the North Island, new Zealand. *J. Hydrol. (New Zealand)* **12**(1), 32–56 (1973).
3. Hewitt, A. E., Balks, M. R. & Lowe, D. J. *The Soils of Aotearoa New Zealand* (Springer Nature, 2021).
4. Orense, R. P., Pender, M. J., Hyodo, M. & Nakata, Y. Micro-mechanical properties of crushable pumice sands. *Géotechnique Lett.* **3** (2), 67–71 (2013).
5. Mesfun, R. T., Quezon, E. T. & Geremew, A. Experimental study of stabilized expansive soil using pumice mixed with lime for subgrade road construction. *Int. J. Research-Granthaalayah.* **7** (7), 118–124 (2019).
6. Chompoorat, T. et al. Cement-based and alkali-activated controlled low-strength materials made from cup lump rubber for use as road materials. *Road. Mater. Pavement Des.* https://doi.org/10.1080/14680629.2024.2409856 (2024).
7. Chompoorat, T., Thepumong, T., Nuaklong, P., Jongvivatsakul, P. & Likitlersuang, S. Alkali-activated controlled low-strength material utilizing high-calcium fly Ash and steel slag for use as pavement materials. *J. Mater. Civ. Eng.* **33** (8), 04021178 (2021).
8. Font, A. et al. Design and properties of 100% waste-based ternary alkali-activated mortars: blast furnace slag, olive-stone biomass Ash and rice husk Ash. *J. Clean. Prod.* **243**, 118568 (2020).
9. Golewski, G. L. Green concrete based on quaternary binders with significant reduced of CO2 emissions. *Energies* **14** (15), 4558 (2021).
10. Abdalqader, A. F., Jin, F. & Al-Tabbaa, A. Development of greener alkali-activated cement: utilisation of sodium carbonate for activating slag and fly Ash mixtures. *J. Clean. Prod.* **113**, 66–75 (2016).
11. Adnan, M., Kumar, S., Garg, N., Gupta, K. K. & Das, S. K. Soil stabilization using waste Bagasse ash and lime: A review. Materials Today: Proceedings. (2023).
12. Ewa, D. E., Egbe, E. A., Ukpata, J. O. & Etika, A. Sustainable subgrade improvement using limestone dust and sugarcane Bagasse Ash. *Sustainable Technol. Entrepreneurship.* **2** (1), 100028 (2023).
13. Sahu, S. K. et al. Untitled-International Journal of Engineering and Advanced.
14. Li, L. et al. Mechanical properties of soil reinforced by fiber and alkaline-activated rice husk Ash, and rainfall erosion model tests. *Sci. Total Environ.* **958**, 178099 (2025).
15. Poorveekan, K., Ath, K., Anburuvel, A. & Sathiparan, N. Investigation of the engineering properties of cementless stabilized Earth blocks with alkali-activated eggshell and rice husk Ash as a binder. *Constr. Build. Mater.* **277**, 122371 (2021).
16. Queiróz, L. C. et al. Alkali-activated system of carbide lime and rice husk for granular soil stabilisation. Proceedings of the Institution of Civil Engineers-Ground Improvement. ;176(5):279 – 94. (2022).

17. Khasib, I. A. & Daud, N. N. N. Physical and mechanical study of palm oil fuel Ash (POFA) based geopolymer as a stabilizer for soft soil. *Pertanika J. Sci. Technol.* **28** (2), 149–160 (2020).
18. Khasib, I. A., Daud, N. N. N. & Nasir, N. A. M. Strength development and microstructural behavior of soils stabilized with palm oil fuel Ash (POFA)-based geopolymer. *Appl. Sci.* **11** (8), 3572 (2021).
19. Pourakbar, S., Asadi, A., Huat, B. B. & Fasihnikoutalab, M. H. Stabilization of clayey soil using ultrafine palm oil fuel Ash (POFA) and cement. *Transp. Geotechnics*. **3**, 24–35 (2015).
20. Santhosh, K. G., Subhani, S. M. & Bahurudeen, A. Sustainable reuse of palm oil fuel Ash in concrete, alkali-activated binders, soil stabilisation, bricks and adsorbent: a waste to wealth approach. *Ind. Crops Prod.* **183**, 114954 (2022).
21. Sukmak, P. et al. Palm oil fuel ash-soft soil geopolymer for subgrade applications: strength and microstructural evaluation. *Road. Mater. Pavement Des.* **20** (1), 110–131 (2019).
22. Lin, J-X. et al. High-strength and high-toughness alkali-activated composite materials: optimizing mechanical properties through synergistic utilization of steel slag, ground granulated blast furnace slag, and fly Ash. *Constr. Build. Mater.* **422**, 135811 (2024).
23. Abdila, S. R. et al. Potential of soil stabilization using ground granulated blast furnace slag (GGBFS) and fly Ash via geopolymerization method: A review. *Materials* **15** (1), 375 (2022).
24. Al-Gharbawi, A. S., Najemalden, A. M. & Fattah, M. Y. Expansive soil stabilization with lime, cement, and silica fume. *Appl. Sci.* **13** (1), 436 (2022).
25. Shi, X. et al. Study on the mechanical properties and microstructure of soil stabilized with alkali-activated slag–steel slag–silica fume. *J. Test. Eval.* **53**(1), 208–225 (2025).
26. Wanare, R., Jayanthi, P. & Iyer, K. K. Experimental study on sustainable stabilization of marine soil with ultrafine slag and activator for controlling its cracking characteristics. *Constr. Build. Mater.* **345**, 128310 (2022).
27. Wang, Z. et al. Investigation and utilization of Alkali-Activated grouting materials incorporating engineering waste soil and fly ash/slag. *Appl. Sci.* **14** (11), 4915 (2024).
28. Dang, M. Q., Kim, Y. & Do, T. M. *Soil Stabilization by Using alkaline-activated Ground Bottom Ash Coupled with Red Mud*p. 800–807 (Congrès International de Géotechnique–Ouvrages–Structures. Springer;, 2017).
29. Kandalai, S. & Patel, A. Alkali activation of red mud and GGBS blends for expansive soil stabilization: strength, durability and leachate studies. *Indian Geotech. J.* :1–26. (2025).
30. Silva, S. S. et al. Use of Red Mud in Soil Stabilization for Pavement Through Alkali Activation. TMS Annual Meeting & Exhibition: Springer; pp. 693–700. (2024).
31. Wan, X., Ding, J., Mou, C., Wang, J. & Zhang, S. Alkali-activated red mud in stabilizing marine dredged clay with low amount of cement. *Eur. J. Environ. Civil Eng.* **27** (16), 4598–4612 (2023).
32. Kong, X., Shi, J., Shen, Y., Zhang, W. & Fu, Y. Sludge-based geopolymer materials: A review. *Int. J. Appl. Ceram. Technol.* **21** (3), 1333–1365 (2024).
33. Pourakbar, S. et al. *Stabilization of Clay Soil Using alkali-activated Sewage Sludge* (Journal of Rock Mechanics and Geotechnical Engineering, 2024).
34. Raoof, B. Z., Abdulkareem, A. H. spsampsps Rajab, A. R. A Promising Use of Water Treatment Sludge–Based Geopolymer for Granular Soil Stabilization. International Conference on Geotechnical Engineering Iraq: Springer; pp. 255 – 70. (2024).
35. Abdeldjouad, L. Clayey soil stabilisation with geopolymerized olivine and glass fibers. *Stud. Eng. Exact Sci.* **5** (2), e9849–e (2024).
36. Emmanuel, E., Yong, L. L., Asadi, A. & Anggraini, V. Full-factorial two-level design in optimizing the contents of olivine and Coir fiber for improving the strength property of a soft marine clay. *J. Nat. Fibers*. **19** (2), 546–561 (2022).
37. Fasihnikoutalab, M. H. et al. Utilization of alkali-activated olivine in soil stabilization and the effect of carbonation on unconfined compressive strength and microstructure. *J. Mater. Civ. Eng.* **29** (6), 06017002 (2017).
38. Idriss, E. et al. Engineering and structural properties of compressed Earth blocks (CEB) stabilized with a calcined clay-based alkali-activated binder. *Innovative Infrastructure Solutions*. **7** (2), 157 (2022).
39. Almalkawi, A. T., Hamadna, S. & Soroushian, P. One-part alkali activated cement based volcanic pumice. *Constr. Build. Mater.* **152**, 367–374 (2017).
40. Kalatehjari, R., Najafi, E. K., Asadi, A. & Brook, M. New Zealand pumicite as a precursor in producing alkaline cement with aluminate-based activators. *Case Stud. Constr. Mater.* **21**, e04008 (2024).
41. Komaei, A. & Saeedi, A. Pumicite-Based geopolymer optimization for sustainable soil stabilization. *J. Mater. Civ. Eng.* **37** (6), 04025141 (2025).
42. Nasir, M., Mahmood, A. H. & Bahraq, A. A. History, recent progress, and future challenges of alkali-activated binders–An overview. *Constr. Build. Mater.* **426**, 136141 (2024).
43. MBIE. *Electricity Statistics. Wellington* (Ministry of Business, Innovation & Employment, 2025).
44. MBIE. *Energy in New Zealand 2024* (Wellington, 2024).
45. Network At-aSB. *Mapping Emissions and Waste Stream Profiles, and Opportunities for Achieving Net-Zero Circular Advanced Manufacturing* (Ministry of Business, Innovation & Employment, 2024).
46. BlueScope Sustainability Report FY2023. Melbourne, Victoria 3000 Australia2023.
47. Chen, Y. et al. Valorization of high-volume crushed waste glass as fine aggregate in foamed geopolymer. *Case Stud. Constr. Mater.* **22**, e04202 (2025).
48. Harrison, E., Berenjian, A. & Seifan, M. Recycling of waste glass as aggregate in cement-based materials. *Environ. Sci. Ecotechnology* **4**, 100064 (2020).
49. Yao, Z., Qin, B., Huang, Z., Ruan, J. & Xu, Z. Green combined resource recycling system for the recycling of waste glass. *ACS Sustain. Chem. Eng.* **9** (21), 7361–7368 (2021).
50. Alqaisi, R., Le, T. M. & Khabbaz, H. Applications of recycled sustainable materials and by-products in soil stabilization. Recent Thoughts in Geoenvironmental Engineering: Proceedings of the 3rd GeoMEast International Congress and Exhibition, Egypt 2019 on Sustainable Civil Infrastructures–The Official International Congress of the Soil-Structure Interaction Group in Egypt (SSIGE): Springer; pp. 91–117. (2020).
51. Hall, B. et al. Best practice expert advice on the use of recycled materials in road and rail infrastructure: part A technical review and assessment. (2022).
52. Redden, R. & Neithalath, N. Microstructure, strength, and moisture stability of alkali activated glass powder-based binders. *Cem. Concr. Compos.* **45**, 46–56 (2014).
53. Rios, L. M. H., Triviño, A. F. H., Villaquirán-Caicedo, M. A. & de Gutiérrez, R. M. Effect of the use of waste glass (as precursor, and alkali activator) in the manufacture of geopolymer rendering mortars and architectural tiles. *Constr. Build. Mater.* **363**, 129760 (2023).
54. Samarakoon, M., Ranjith, P. & De Silva, V. Effect of soda-lime glass powder on alkali-activated binders: rheology, strength and microstructure characterization. *Constr. Build. Mater.* **241**, 118013 (2020).
55. Xiao, R. et al. Evaluation of glass powder-based geopolymer stabilized road bases containing recycled waste glass aggregate. *Transp. Res. Rec.* **2674** (1), 22–32 (2020).
56. Bianco, I., Tomos, B. A. D. & Vinai, R. Analysis of the environmental impacts of alkali-activated concrete produced with waste glass-derived silicate activator–A LCA study. *J. Clean. Prod.* **316**, 128383 (2021).
57. El-Seidy, E. et al. Lightweight alkali-activated materials and ordinary Portland cement composites using recycled Polyvinyl chloride and waste glass aggregates to fully replace natural sand. *Constr. Build. Mater.* **368**, 130399 (2023).

58. Vafaei, M. & Allahverdi, A. High strength geopolymer binder based on waste-glass powder. *Adv. Powder Technol.* **28** (1), 215–222 (2017).
59. Xiao, R. et al. Strength, microstructure, efflorescence behavior and environmental impacts of waste glass geopolymers cured at ambient temperature. *J. Clean. Prod.* **252**, 119610 (2020).
60. Gao, X. et al. Performance of fly ash-based geopolymer mortars with waste cathode ray tubes glass fine aggregate: A comparative study with cement mortars. *Constr. Build. Mater.* **344**, 128243 (2022).
61. Toniolo, N. et al. Novel geopolymers incorporating red mud and waste glass cullet. *Mater. Lett.* **219**, 152–154 (2018).
62. Burciaga-Díaz, O., Durón-Sifuentes, M., Díaz-Guillén, J. & Escalante-García, J. Effect of waste glass incorporation on the properties of geopolymers formulated with low purity Metakaolin. *Cem. Concr. Compos.* **107**, 103492 (2020).
63. Tho-In, T., Sata, V., Boonserm, K. & Chindaprasirt, P. Compressive strength and microstructure analysis of geopolymer paste using waste glass powder and fly Ash. *J. Clean. Prod.* **172**, 2892–2898 (2018).
64. Shoaei, P., Ameri, F., Musaeei, H. R., Ghasemi, T. & Cheah, C. B. Glass powder as a partial precursor in Portland cement and alkali-activated slag mortar: A comprehensive comparative study. *Constr. Build. Mater.* **251**, 118991 (2020).
65. Sun, K., Ali, H. A., Xuan, D., Ban, J. & Poon, C. S. Utilization of APC residues from sewage sludge incineration process as activator of alkali-activated slag/glass powder material. *Cem. Concr. Compos.* **133**, 104680 (2022).
66. You, I., Yoo, D-Y., Lee, S-J., Lee, Y. & Zi, G. A combination of liquid–crystal display glass powder and slag in alkali-activated material. *Constr. Build. Mater.* **369**, 130527 (2023).
67. Zhang, L. & Yue, Y. Influence of waste glass powder usage on the properties of alkali-activated slag mortars based on response surface methodology. *Constr. Build. Mater.* **181**, 527–534 (2018).
68. Liu, G., Florea, M. & Brouwers, H. Characterization and performance of high volume recycled waste glass and ground granulated blast furnace slag or fly Ash blended mortars. *J. Clean. Prod.* **235**, 461–472 (2019).
69. Santana-Carrillo, J., Burciaga-Díaz, O. & Escalante-Garcia, J. Blended limestone-Portland cement binders enhanced by waste glass based and commercial sodium silicate-Effect on properties and CO2 emissions. *Cem. Concr. Compos.* **126**, 104364 (2022).
70. Si, R., Dai, Q., Guo, S. & Wang, J. Mechanical property, nanopore structure and drying shrinkage of metakaolin-based geopolymer with waste glass powder. *J. Clean. Prod.* **242**, 118502 (2020).
71. Guo, W. et al. Effects of various curing methods on the compressive strength and microstructure of blast furnace slag-fly ash-based cementitious material activated by alkaline solid wastes. *Constr. Build. Mater.* **357**, 129397 (2022).
72. Khan, M. N. N., Kuri, J. C. & Sarker, P. K. Effect of waste glass powder as a partial precursor in ambient cured alkali activated fly Ash and fly Ash-GGBFS mortars. *J. Building Eng.* **34**, 101934 (2021).
73. Maldonado-Alameda, A., Mañosa, J., López-Montero, T., Catalán-Parra, R. & Chimenos, J. High-porosity alkali-activated binders based on glass and aluminium recycling industry waste. *Constr. Build. Mater.* **400**, 132741 (2023).
74. Pitarch, A. et al. Reutilisation of hazardous spent fluorescent lamps glass waste as supplementary cementitious material. *Constr. Build. Mater.* **292**, 123424 (2021).
75. Marathe, S., Mithanthaya, I., Mithun, B., Shetty, S. & Akarsh, P. Performance of slag-fly Ash based alkali activated concrete for paver applications utilizing powdered waste glass as a binding ingredient. *Int. J. Pavement Res. Technol.* **14**, 196–203 (2021).
76. Bilondi, M. P., Toufigh, M. M. & Toufigh, V. Experimental investigation of using a recycled glass powder-based geopolymer to improve the mechanical behavior of clay soils. *Constr. Build. Mater.* **170**, 302–313 (2018).
77. Baldovino, J. J., Izzo, R. L., Rose, J. L. & Domingos, M. D. Strength, durability, and microstructure of geopolymers based on recycled-glass powder waste and dolomitic lime for soil stabilization. *Constr. Build. Mater.* **271**, 121874 (2021).
78. Más-López, M. I., García del Toro, E. M., Luizaga Patiño, A. & García, L. J. M. Eco-friendly pavements manufactured with glass waste: physical and mechanical characterization and its applicability in soil stabilization. *Materials* **13** (17), 3727 (2020).
79. Onitsuka, K. & Shen, J. Evaluation of lime-stabilized Ariake clay with foaming waste glass as pavement materials. *Int. J. Pavement Eng.* **1** (1), 35–47 (1999).
80. Hamouda, A. A. & Akhlaghi Amiri, H. A. Factors affecting alkaline sodium silicate gelation for in-depth reservoir profile modification. *Energies* **7** (2), 568–590 (2014).
81. Turner, L. K. & Collins, F. G. Carbon dioxide equivalent (CO2-e) emissions: A comparison between geopolymer and OPC cement concrete. *Constr. Build. Mater.* **43**, 125–130 (2013).
82. Alberici, S., de Beer, J., van der Hoorn, I. & Staats, M. Fly Ash and blast furnace slag for cement manufacturing. *BEIS Res. Paper*. **19**, 1–35 (2017).
83. ASTM-C136-06. *Annual Book of ASTM Standards. Standard Test Method for Sieve Analysis of Fine and Coarse Aggregates* (ASTM International, 2006).
84. ASTM-D7928-21. *Annual Book of ASTM Standards. Standard Test Method for Particle-Size Distribution (Gradation) of Fine-Grained Soils Using the Sedimentation (Hydrometer) Analysis* (ASTM International, 2021).
85. Marks, S., Larkin, T. & Pender, M. The dynamic properties of a pumiceous sand. *Bull. New. Z. Soc. Earthq. Eng.* **31** (2), 86–102 (1998).
86. ASTM-D698. *Annual Book of ASTM Standards. Standard Test Methods for Laboratory Compaction Characteristics of Soil Using Standard Effort* (ASTM International, 2007).
87. ASTM-C109/C109M-24. *Annual Book of ASTM Standards. Standard Test Method for Compressive Strength of Hydraulic Cement Mortars (Using 50 mm [2 in] Cube Specimens* (ASTM International, West Conshohocken, 2024).
88. ASTM-D1557-12. *Annual Book of ASTM Standards. Standard Test Methods for Laboratory Compaction Characteristics of Soil Using Modified Effort, (56,000 ft-lbf/ft^3 (2,700 kN-m/m^3))* (ASTM International, West Conshohocken, 2021).
89. ASTM-D1883-21. *Annual Book of ASTM Standards. Standard Test Method for California Bearing Ratio (CBR) of Laboratory-Compacted Soils* (ASTM International, West Conshohocken, 2021).
90. Rai, P. et al. Effect of fly Ash and cement on the engineering characteristic of stabilized subgrade soil: an experimental study. *Geofluids* **2021** (1), 1368194 (2021).
91. Rivera, J., Orobio, A., de Gutiérrez, R. M. & Cristelo, N. Clayey soil stabilization using alkali-activated cementitious materials. *Materiales De Construcción*. **70** (337), e211–e (2020).
92. Pourakbar, S., Asadi, A., Huat, B. B. & Fasihnikoutalab, M. H. Soil stabilisation with alkali-activated agro-waste. *Environ. Geotechnics*. **2** (6), 359–370 (2015).
93. Davidovits, J. Geopolymer chemistry and applications. Institut Géopolymère, Geopolymer Institute, Saint-Quentin, France. ISBN 2-951-14820-1-9; (2008).
94. Zhao, Z., Xiao, F. & Amirkhanian, S. Recent applications of waste solid materials in pavement engineering. *Waste Manage.* **108**, 78–105 (2020).
95. Provis, J. L., Yong, C. Z., Duxson, P. & van Deventer, J. S. Correlating mechanical and thermal properties of sodium silicate-fly Ash geopolymers. *Colloids Surf., A*. **336** (1–3), 57–63 (2009).
96. Xu, H. & van Deventer, J. S. The effect of alkali metals on the formation of geopolymeric gels from alkali-feldspars. *Colloids Surf., A*. **216** (1–3), 27–44 (2003).
97. Miraki, H. et al. Clayey soil stabilization using alkali-activated volcanic Ash and slag. *J. Rock Mech. Geotech. Eng.* **14** (2), 576–591 (2022).
98. Görhan, G. & Kürklü, G. The influence of the NaOH solution on the properties of the fly ash-based geopolymer mortar cured at different temperatures. *Compos. Part. B: Eng.* **58**, 371–377 (2014).

99. Singh, G. B. & Subramaniam, K. V. Evaluation of sodium content and sodium hydroxide molarity on compressive strength of alkali activated low-calcium fly Ash. *Cem. Concr. Compos.* **81**, 122–132 (2017).
100. Zribi, M., Samet, B. & Baklouti, S. Effect of curing temperature on the synthesis, structure and mechanical properties of phosphate-based geopolymers. *J. Non-cryst. Solids.* **511**, 62–67 (2019).
101. Cristelo, N., Rivera, J., Miranda, T. & Fernández-Jiménez, A. Stabilisation of a plastic soil with alkali activated cements developed from industrial wastes. *Sustainability* **13** (8), 4501 (2021).
102. Feng, S. et al. The influence of CaO and MgO on the mechanical properties of alkali-activated blast furnace slag powder. *Materials* **15** (17), 6128 (2022).
103. Frare, A., Luz CAd, M. & MHFd, Pereira Filho, J. I. Study of SiO2/Al2O3 and CaO/SiO2 relationships in alkali-activated cements. *Revista IBRACON De Estruturas E Materiais*. **17** (3), e17313 (2024).
104. Walker, R. & Pavia, S. Behaviour and properties of lime-pozzolan pastes. in *Eighth International Masonry Conference held in Dresden* (ed. Jäger, W. & Haseltine, B.) 353–364. 4th to 7th July 2010 (2010).
105. Shelby, J. E. Properties and structure of soda-lime aluminosilicate glasses. *J. Appl. Phys.* **66** (5), 1947–1950 (1989).
106. Jantzen, C. M. & Plodinec, M. Thermodynamic model of natural, medieval and nuclear waste glass durability. *J. Non-cryst. Solids.* **67** (1–3), 207–223 (1984).
107. Dimas, D., Giannopoulou, I. & Panias, D. Polymerization in sodium silicate solutions: a fundamental process in geopolymerization technology. *J. Mater. Sci.* **44** (14), 3719–3730 (2009).

Acknowledgements
The authors gratefully acknowledge Yousef Adeeb Chamachaei, Sara Bayandor, and Ava Asadi for their invaluable assistance throughout this research.

Author contributions
All authors contributed to the study's conception and design. Material preparation and data collection were performed by R.K. Result analysis was performed by all authors. The first draft of the manuscript was written by R.K. and E.K.N. and all authors commented on previous versions of the manuscript. All authors read and approved the final manuscript.

Funding
This work was supported by Waka Kotahi Hoe ki angitū - Innovation Fund (Grant number HKA1.1.1).

Declarations

Competing interests
The authors declare no competing interests.

Additional information
Correspondence and requests for materials should be addressed to R.K.

Reprints and permissions information is available at www.nature.com/reprints.

Publisher's note Springer Nature remains neutral with regard to jurisdictional claims in published maps and institutional affiliations.